Correlation between excitation energy and nucleonic phase space in the projectile fragmentation process

C. Beşliu,[1,*] D. Felea,[2,†] V. Topor-Pop,[2,‡] A. Gheaţă,[2] I. S. Zgură,[2] Al. Jipa,[1] and R. Zaharia[1]
[1]*Faculty of Physics, University of Bucharest, Bucharest-Măgurele, P.O. Box MG 11, Romania*
[2]*Institute of Space Sciences, Bucharest-Măgurele, P.O. Box MG 36, Romania*
(Received 6 November 1998; published 23 July 1999)

Using the former results and analyzing the quantitative discrepancies between the experimental data and present theories concerning the projectile fragmentation process we propose an improvement on Goldhaber formula. We want therefore to sustain the idea that the projectile fragmentation process is not as fast as it was supposed to be from the very beginning. The process would be governed by the distribution of nucleon momenta in the projectile shortly after the collision occurred. We used in our analysis protons from the ^{4}He fragmentation when colliding ^{7}Li target at 4.5 GeV/c per nucleon incident momentum, protons detected by the 2 m streamer chamber from SKM 200 spectrometer as well as ^{40}Ar ($E_{\rm inc}=213$ MeV/nucleon)$+^{12}$C data used in previous papers. Our purpose was to demonstrate that in order to proceed in analyzing the projectile fragmentation process at intermediate and high energies one has to take into account the dependence of σ_0 on the apparent temperature of projectile nucleus soon after the collision took place. The generalized Bertsch correction for all light up to medium projectile nuclei and fragments is used and the total number of spatial correlations between identical nucleons (in the same state of spin and isospin) having anticorrelated momenta is evaluated. Considering all those criteria as well as the projectile excitation hypothesis, apparent temperature values reasonably close to the separation energies of the considered fragments per number of fragments were found. [S0556-2813(99)01408-9]

PACS number(s): 25.70.Mn, 25.60.Gc, 24.10.Pa, 25.10.+s

I. INTRODUCTION AND BACKGROUND

The problem of explaining the mechanism of projectile fragmentation at high energies was initiated about 30 years ago and since then more refined experimental data and new theoretical treatments of this kind of process have been made.

First experimental results [1] suggested that the projectile breakup is a fast process governed by Gaussian type momentum distribution of the nucleons in the projectile before the collision took place [2]:

$$f(P)\propto\exp[-(P/\sqrt{2}m_\pi c)^2], \tag{1}$$

where $\sigma\approx m_\pi c=139$ MeV/c, and $\sigma\neq\sigma(A_{\rm fragment})$.

It was further shown [3–5] that the dispersion of the longitudinal momentum values in the frame where projectile is in rest is a function of the mass number of the fragment K in a manner well-fitted by a parabolic expression:

$$\sigma^2=\sigma_0^2\frac{K(A-K)}{A-1}. \tag{2}$$

Here, K is the mass number of fragment and A is the mass number of projectile. The variance σ_0^2 appear as a constant, the experimental value found being $\sigma_{0\rm exp}\approx 90$ MeV/c.

If the projectile could pass a rough thermal equilibrium state instead of sudden liberation of virtual fragments, a similar equation to (2) would be obtained [3]:

$$\sigma^2=m_N T\frac{K(A-K)}{A}, \tag{3}$$

where m_N is the nucleon mass and the temperature T is corresponding to an excitation energy close to mean nucleon binding energy (≈ 9 MeV). Still, there was a discrepancy between the experimental values and theoretical ones for σ_0 (for ^{40}Ar and $K=20$: $\sigma_{0\rm theor}\approx 1.32\sigma_{0\rm exp}$ [6]).

The diminution of the dispersion was achieved by including Pauli correlation (Ref. [6]) (e.g., for ^{40}Ca dispersion is reduced by 37% compared to 31.5% measured reduction). Also, by presuming that the fragment is a Fermi gas [7]. The results are qualitatively improved, showing the dependence of $\sigma_{\rm o}$ on the mass number of the fragment, including a particular behavior at $A/2$. However, the predicted fragment momentum distributions were narrower than those observed, sometimes by a large degree. By applying a kinematical semiclassical model [8] the width of the momentum distribution of a fragment was found to be sensitive to the single-particle distribution but the quantitative difference with the experiment still remains. For heavy projectiles broader experimental widths could be observed than for light and medium ones (Refs. [9,10]).

Taking into account that the modes of projectile fragmentation are independent of the target nucleus [11–13], the above discrepancy could be understood in the view that the projectile nucleus is not a simple spectator [14] and that the projectile breakup is not a cold process [15] as it was assumed from the very beginning [3].

*Electronic address: besc@scut.fizica.unibuc.ro
†Electronic address: felea@venus.nipne.ro
‡Present address: Physics Department, McGill University, Montreal, Canada.

The mechanism of the transfer of energy and momentum to the projectile prefragment was described in [9] ($E_{\rm inc}$ = 1200 MeV/nucleon) and in [16] ($E_{\rm inc}$ = 600 MeV/nucleon). Using temperature measurements performed by the ALADIN group, one can find that the density of the nuclear system and the excitation energy received by the spectators during collision could be dominated by dynamical processes as shown by the IN2P3 Collaboration [16]. Their behavior could as well be explained using thermodynamical models, based on the assumption that the system passes a state of thermal equilibrium [17].

By applying the Fermi gas formula, an apparent temperature around 5.5 MeV was obtained [16], although the main conclusion was that the system included in that analysis Au+Au ($E_{\rm inc}$ = 600 MeV/nucleon) might not be in equilibrium. Apart from the aforementioned assumption made by Goldhaber on the possibility of a thermal equilibrium state to be established [3], several methods have been developed in order to estimate the excitation energy transferred to the projectile during collision [18–22]. By using the double ratios of hydrogen, helium, and lithium isotopic yields in ^{197}Au + ^{197}Au central collisions, breakup temperatures from 5 MeV to 12 MeV were found, corresponding to an incident energy from 50 to 200 MeV/nucleon [23]. Similar values were derived, independently of the bombarding energy, from the correlated yields of light-particle coincidences [24–26].

On the other hand, under the assumption that the thermal equilibrium of the system could be achieved, the linear dependencies between the variance of the fragment velocity spectra and the fragment mass offer apparent temperature values around 30 MeV [13].

These two kinds of temperature values could be related by applying the single particle model as shown recently by Bauer in [15].

The present study shows that in order to proceed in analyzing the projectile fragmentation process at high energies, we have to take into account the dependence of $\sigma_{\rm o}$ on the apparent temperature of projectile nucleus after the collision took place as predicted earlier [15]. The projectile fragmentation would still be a fast process, yet not as fast as it was supposed to be from the very beginning [3]. The process would be governed by the Fermi distribution of nucleon momenta in the excited projectile. Although we used a statistical method combined with Pauli exclusion principle we formulate our assumptions in the terms of an ''apparent temperature'' because the intrinsic mechanism of the energy transfer to the projectile is still unknown.

In Sec. II of the present paper we present the experimental setup. Several experimental results are also discussed. Section III describes the formalism used. Because the fragment is a Fermi gas the Murphy hypothesis [7] will be taken into account in Sec. III A. We will consider the Bertsch technique [6] based on Pauli correlations for all light up to medium projectile nuclei and fragments in Sec. III B. An evaluation method of the total number of possible spatial combinations between identical nucleons (in the same state of spin and isospin) having anticorrelated momenta will be proposed in the same section. In Sec. III C the projectile excitation hypothesis as suggested by Bauer [15] will be applied. The connection between the obtained apparent temperatures and the nucleonic phase space will be displayed and some comments will be presented in Sec. IV. Section V summarizes and concludes the paper.

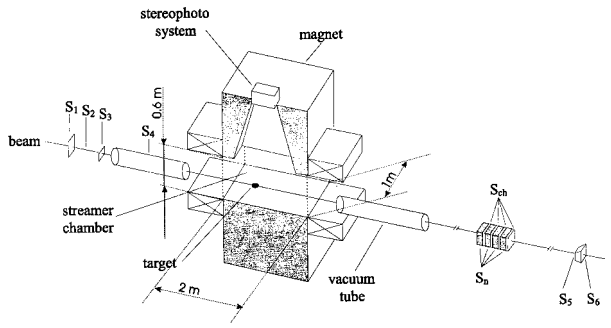

FIG. 1. The SKM 200 spectrometer from JINR Dubna (Russia).

II. EXPERIMENTAL SETUP AND RESULTS

We used in the present analysis ^{4}He nuclei accelerated at the JINR Dubna Synchrophasotron, at 4.5 GeV/c per nucleon momentum. The detection device is the SKM 200 spectrometer, shown schematically in Fig. 1 [27–29]. This spectrometer has a streamer chamber with the following dimensions 2 m×1 m×0.6 m, filled with pure neon under atmospheric pressure for these experiments and placed in a magnetic field of 0.8 T. Solid targets in the form of thin disks (in the case of Li target the thickness was 1.6 g/cm^2) were mounted inside the chamber. The high voltage (500 kV/pulse, 10.5 ns length of pulse) is supplied by a Marx generator. A stereo-photographic system with three cameras allows us to record the experimental information on high sensibility films (in the case of ^{4}He+^{7}Li exposures two objectives were used).

The streamer chamber can be triggered with two systems of scintillation. The minimum bias triggering system for ''inelastic'' events, consisting of two sets of counters mounted upstream and downstream the streamer chamber, selected inelastic interactions of incident nuclei within the chamber [$T(\theta_{\rm ch}=0°,\theta_n=0°)$]. Here, $\theta_{\rm ch}$ and θ_n are the minimum values of the emission angles accepted for the charged particles, fragments of the projectile nucleus with momenta higher than 3.5 GeV/c per nucleon (for these experiments), known as stripping particles, and for the neutrons, respectively. The trigger efficiency was ≈99% for one charged particle and ≈80% for one neutron. For inelastic collisions of ^{4}He all charged secondaries having $p/z>3.5$ GeV/c were measured regardless of the emission angle. In the present analysis only the most statistically significant sample $T(0,0)$ was used. The triggering system selected required projectile nuclei from a primary beam with an efficiency higher than 99%. The multiplicity distributions for inelastic interactions were corrected as described in [30].

The ''central'' triggering system has in the downstream part scintillation veto counters, registering a projectile and its charged fragments [$T(\theta_{\rm ch}>0°,\theta_n\geqslant 0°)$]. A trigger bias for central collisions is activated whenever a secondary particle from a central collision hits the veto counters and simulates a

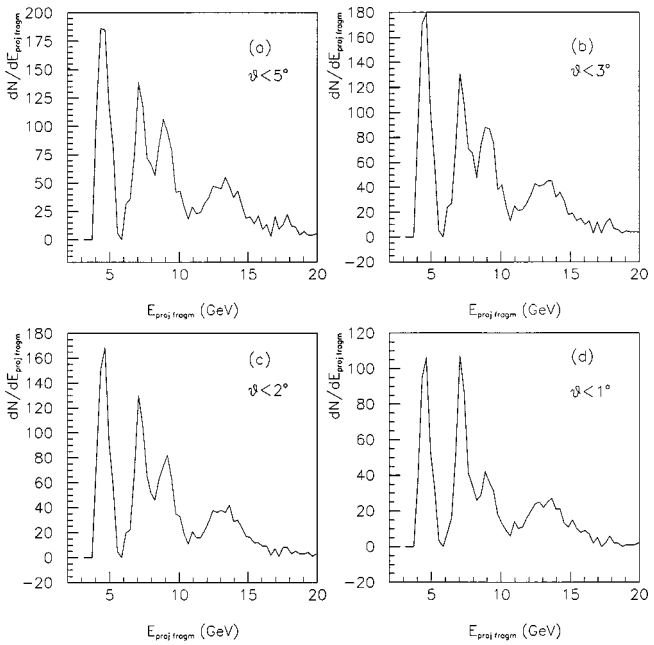

FIG. 2. The total energy distribution in the laboratory system for positive particles with momenta higher than 3.5 GeV/c per nucleon, for ^{4}He+^{7}Li collisions at 4.5 GeV/c per nucleon incident momentum.

projectile-nucleus fragment. The effect was studied by simulating trajectories of secondary particles generated within the framework of the cascade model [31].

The geometry of the experimental setup and magnetic field distribution were taken into account. The corrections due to secondary interactions within a solid target turned out to be significant only for the Li target. The data on the multiplicity for ^{4}He+^{7}Li interactions were corrected for this bias [30].

The experimental data are obtained by scanning, measuring, and performing geometrical reconstruction. Corrections for scanning losses originate from two sources: scanning inefficiency ($\approx 2\%$) and losses of the tracks with a small projection length (which may be screened by the target container or a flash around the vertex) and/or a small curvature ($\approx 1-4\%$). For these experiments the absolute error in the emission angle of the stripping particles is around 10 mr for all angles, and the relative error in momentum is about 8% for all momenta.

The SKM 200 spectrometer is detecting for charged objects only the momenta and the emission angles. The charges of the secondary particles were determined in the first phase by visual examination of the track ionization on the film. However, one cannot apply only this criterion for identifying the nuclear fragments because the estimation of the degree of ionization by ranging the streamer density is not as rigorous as for the bubble chamber. This is due to the instability of the streamer shape that leads to a large dispersion in evaluating the trace density. In exchange, a kinematical method was chosen. By observing the general distribution of the total energy, one could find for different cuts in the polar angle of the fragments [Figs. 2(a)–2(d)] four Gaussian shaped peaks, centered approximately on 4.5, 6.7, 9.0, and 13.5 GeV per nucleon, corresponding to the kinematical zones associated to protons (forward and backward in the c.m.s.) [32], deuterons, and tritons (or ^{3}He), respectively. The yields of these fragments are given in Table I.

TABLE I. The percentages of protons, deuterons, and tritons (^{3}He) for ^{4}He+^{7}Li interactions at 4.5 GeV/c per nucleon incident momentum.

$\theta(^\circ)$	N_{1_p}/N_{ALL} (%)	N_{2_d}/N_{ALL} (%)	N_{3_t}/N_{ALL} (%)
3	59.99	24.21	15.80
5	65.55	21.34	13.11
10	70.46	18.61	10.93
>10	72.00	17.66	10.34

Moreover, we have used the relativistic quantum molecular dynamics model (RQMD 2.4) for several physical hypotheses that fit best the Monte Carlo simulated distributions with the experimental ones. Other positive particles, like π^+ and K^+, were observed. However, the contamination percentage with these particles having momenta higher than 3.5 GeV/c to the proton momenta distributions was found to be insignificant for our study (i.e., 0.03–0.06 %).

We start our analysis by following a Monte Carlo simulation technique [33,34] to determine the Fermi radius of helium projectile under the Goldhaber breakup hypothesis [3]. Despite using the Woods-Saxon form factor for very light projectile nuclei, the obtained value ($r_{F_{\mathrm{He}}} \approx 1.6$ fm) looks unrealistic. One could observe (Fig. 3) an experimental Gaussian distribution of longitudinal proton momenta in the projectile rest frame for ^{4}He+^{7}Li interactions at $p_{\mathrm{inc}} = 4.5$ GeV/c per nucleon. This is broader than the analogous Monte Carlo simulated distribution having $r_{F_{\mathrm{He}}} \approx 2.6$ fm predicted by the interpolation spline function on the Moniz set of experimental data (Ref. [35]).

A preliminary remark might indicate, even if we do not use a transverse momentum method, that after collision an unnegligible amount of energy from nucleon-nucleon scattering was transferred to the projectile nucleus. This is reflected by a broader dispersion than for the nonexcited projectile case (Ref. [3]). The aforementioned remark could be strengthened by the first microscopic calculation of the spectator fragmentation [16]. By studying Au+Au collisions at 600 MeV/nucleon, Gossiaux *et al.* found that the excitation energy and the density of the nuclear system are dominated by dynamical processes. By applying SACA (simulated annealing cluster algorithm) instead of MST (minimum spanning tree) they found that the interaction between projectile and target increases the width of the momentum distributions considerably in comparison with that obtained from a simple Goldhaber model (for $K=5$): $\sigma(p_x)_{\mathrm{SACA}}[t \geqslant 200$ fm/$c]/\sigma(p_x)_{\mathrm{Goldhaber}}[t=0$ fm/$c] \approx 0.08$ GeV/c/0.0469 GeV/c $=1.71$. For comparison, we have obtained for protons in ^{4}He+^{7}Li interactions at $p_{\mathrm{inc}}=4.5$ GeV/c per nucleon (Fig. 3): $\sigma(p_z)[T \neq 0]/\sigma(p_z)[T=0] \approx 0.1064$ GeV/c/0.0673 GeV/c $=1.58$.

A fit of Eq. (2) to the ALADIN data [13] yielding a Fermi momentum as compared with that extracted from electron

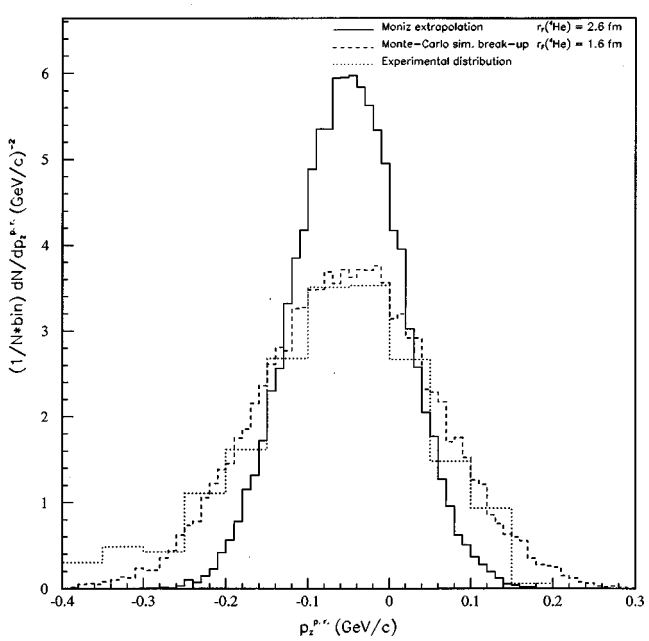

FIG. 3. The experimental Gaussian distribution of the longitudinal proton momenta in the projectile rest frame (p.r.) for ^{4}He $+^7$Li interactions at $p_{\rm inc}=4.5$ GeV/c per nucleon compared with Monte Carlo simulated similar distribution having $r_{F_{\rm He}}\approx 2.6$ fm predicted by the interpolation spline function on the Moniz set of experimental data. For comparison is given also the Monte Carlo distribution that fits best the experimental one. The Fermi radius obtained is too small even though Woods-Saxon form factor for very light projectile nuclei is applied.

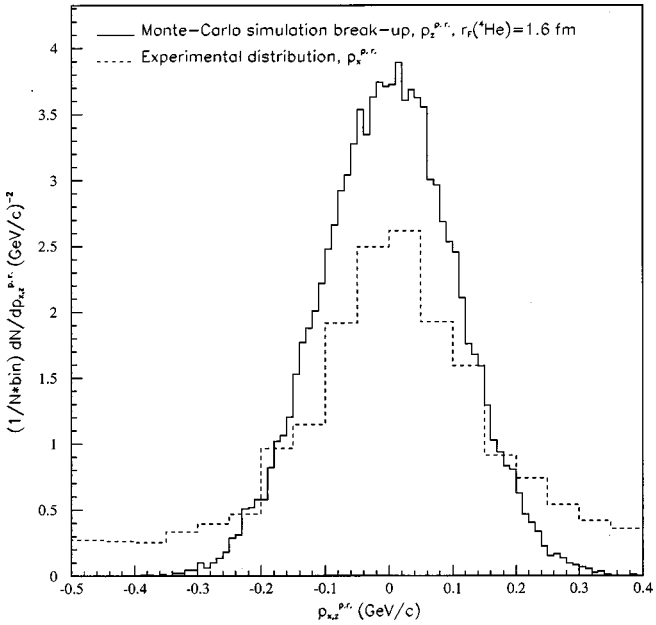

FIG. 4. The experimental distribution of the transverse components p_x of proton momenta in the fragmenting nucleus rest frame (p.r.) and the Monte Carlo normal distributions of the associated longitudinal components p_z for ^{4}He$+^7$Li collisions at $E_{\rm inc}=4.6$ GeV per nucleon.

scattering gives $(p_F[\exp]-p_F[T=0])/p_F[T=0]\approx 50\%$. Using instead for our experimental data the Fermi radius of the helium projectile nucleus as an input parameter in the Monte Carlo simulations as shown earlier (Fig. 3), and taking into account that the momentum is in inverse proportion to the nucleus radius in the Fermi model, one can obtain $(r_F[T=0]-r_F[T\neq 0])/r_F[T\neq 0]\approx 62.5\%$.

One can also notice larger widths of the distributions of the transverse components p_x and p_y in the fragmenting nucleus rest frame compared to the similar normal distributions of the longitudinal component p_z (see Fig. 4). This aspect seems to indicate that the transverse momentum analysis could be used in evaluating both the degree of thermalization for participant zone of the interaction (the so-called ''fire-ball'') and the degree of excitation for the projectile spectators.

The topology was found to play an important role in the projectile fragmentation as shown in [12]. In order to verify this assumption one can determine the longitudinal momentum distribution widths σ_0 for different cuts in the total energy of the residual products of the projectile found within the fragmentation cone [see, e.g., Figs. 5(a)–5(d)]. These cuts could offer an estimator of the projectile-target overlap. For different forward polar angles from 0.5° to 10° we found that σ_0 is sensitive to the excitation degree of the projectile before breakup (Fig. 6).

III. FORMALISM

A. Murphy hypothesis

The Murphy correction factor for any fragment with K nucleons can be derived by evaluating the number of projec-

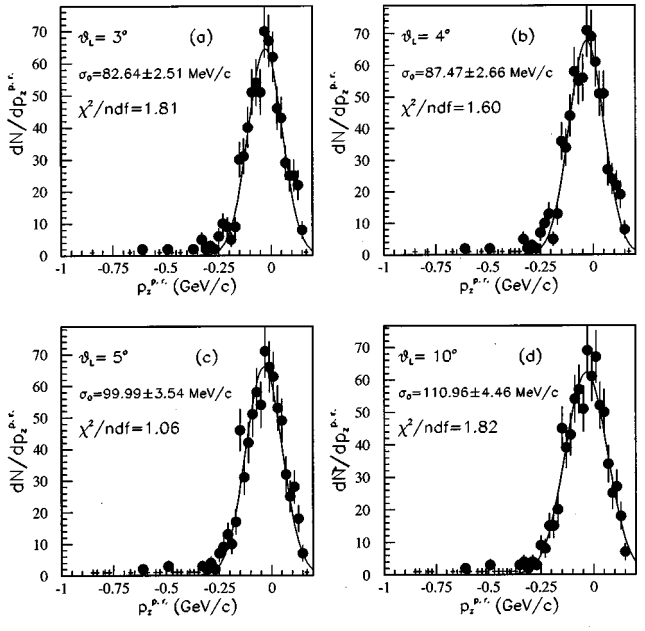

FIG. 5. The experimental distributions of the longitudinal proton momenta in the projectile rest frame (p.r.) for ^{4}He$+^7$Li interactions at $p_{\rm inc}=4.5$ GeV/c. The solid line is a Gaussian fit for a total energy per event $3.5\leqslant\Sigma_{\rm proj\ fragm}E(\theta<\theta_L)\leqslant 5.9$ GeV and for four choices of the maximum polar angle θ_L of the emitted projectile fragments.

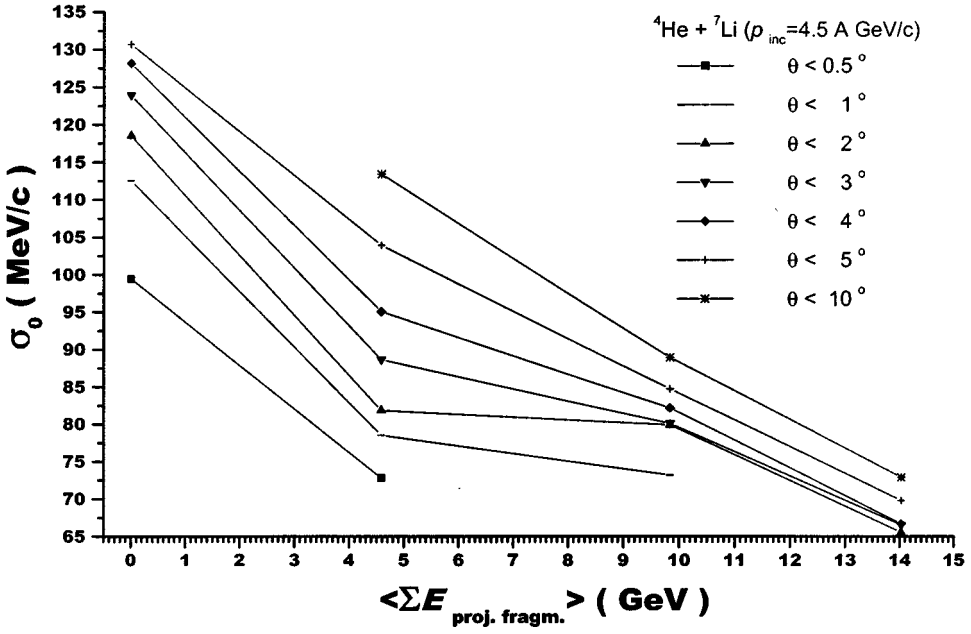

FIG. 6. The dependence of the distribution width of the protons momenta σ_0 measured in the helium rest frame (p.r.) with the total energy of the residual fragments of the projectile within different solid angles from 0.5° to 10°. The lines are drawn only to guide the eye.

tile states available to produce fragments $N(P_K)$ under no restriction and the same number $N'(P_K)$ considering that the fragment is also a Fermi gas (Ref. [7]):

$$\left(\frac{w'}{w}\right)_M = \frac{N'(P_K)}{N(P_K)} = \frac{\sigma'(P_K)}{\sigma(P_K)}. \tag{4}$$

We computed the dispersions of the above distributions (Figs. 7 and 8) by calculating the nucleon momentum in the projectile rest frame p_i (5), its projection on the incident axis (6) and the angle $\beta_{ij}=(\widehat{\vec{P}_K,\vec{p}_i})$ (7). Therefore, we took as parameters the nucleon momentum in the fragment K's rest frame p_j, the total momentum P_K of the fragment K in the projectile rest frame, and the angle $\alpha_j=(\widehat{\vec{P}_K,\vec{p}_j})$:

$$p_i = \sqrt{\left(\frac{P_K}{K}\right)^2 + p_j^2 + 2\left(\frac{P_K}{K}\right) p_j \cos\alpha_j}, \tag{5}$$

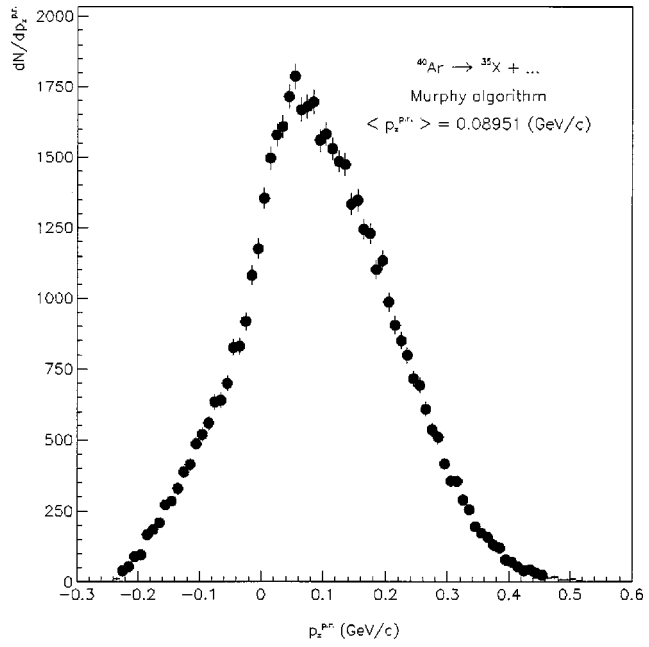

FIG. 7. The Monte Carlo distribution of the nucleon momenta projected on the incident axis obtained under Murphy hypothesis that the residual nucleus is also a Fermi gas—$\langle p_z\rangle \approx 90$ MeV/c.

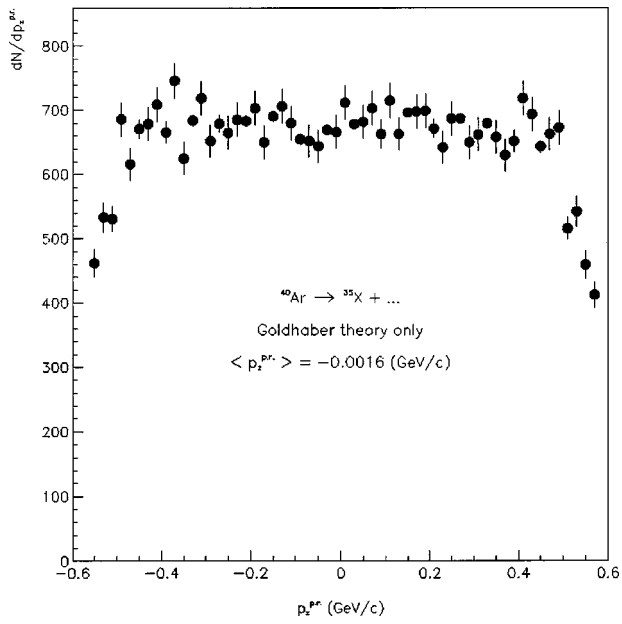

FIG. 8. The Monte Carlo random distribution of the longitudinal nucleon momenta obtained when no hypothesis are applied (Goldhaber theory)—$\langle p_z\rangle \approx 1.5$ MeV/c.

$$p_{z_i} = p_i \cos\beta_{ij} = \frac{P_K}{K} + p_j \cos\alpha_j , \tag{6}$$

$$\beta_{ij} = \arctan\left(\frac{p_j \sin\alpha_j}{\frac{P_K}{K} + p_j \cos\alpha_j} \right). \tag{7}$$

We obtained for each studied fragment the probability distributions for 50 000 events by subtracting the contribution of the Gaussian distribution. The longitudinal momentum distribution in the projectile rest frame has an altered shape due to the restriction of the momentum conservation and a mean value far remote from zero ($\langle p_z \rangle \approx 90$ MeV/c; Fig. 7), while the values from the distribution unaffected by Murphy hypothesis are random distributed, as expected ($\langle p_z \rangle \approx 1.5$ MeV/c; Fig. 8).

B. The generalized Bertsch correction factor

As the Bertsch correction formula (9) concerns only the projectile nuclei and breakup fragments having completed orbits a_A and respectively a_K ($A = 4a_A; K = 4a_K$), in particular only for the ^{40}Ca incident nucleus and for $K = 20$ fragment were given the results [6].

In order to obtain the generalized Bertsch correction for light up to medium nuclei where the harmonic oscillator wave function can describe the nucleons motion in the projectile nucleus, we have to evaluate the total number of spatial correlations between identical nucleons within the same state of spin and isospin and having anticorrelated momenta. Considering as Bertsch did (Ref. [6]) that the experiment measures the momentum on z incident direction in the disintegrating nucleus rest frame, let the operator O have as eigenvalues the longitudinal components of nucleon momenta:

$$O = p_z f(x,y). \tag{8}$$

In a quantical description the dispersion of the longitudinal momenta for a residual fragment with a number of a orbits filled up with nucleons has the known form [6]

$$\left\langle \Psi \left| \left(\sum_{i=1}^{a} O_i \right)^2 \right| \Psi \right\rangle = 4a\langle \Psi | O_i^2 | \Psi \rangle + 4A_a^2 \langle \Psi | O_i O_j | \Psi \rangle_{\mathrm{id}} + 12a^2 \langle O_i O_k \rangle_{\mathrm{non}} . \tag{9}$$

The O^2 operator applies on the wave function of the projectile that could be separated in the Cartesian coordinates. One can evaluate the matrix elements up to a normalization factor by introducing the projection operator:

$$\Psi = \prod_{n=1}^{a} \varphi_{n_x}(x) \varphi_{n_y}(y) \varphi_{n_z}(z), \tag{10}$$

where $n \equiv (n_x, n_y, n_z)$ represents the set of quantum numbers of the occupied orbits.

In order to obtain the well-known factor N_G, one has to follow Goldhaber theory [3] and consequently to avoid the Pauli correlations between nucleons in the first phase:

$$N_G = \frac{K(A-K)}{A-1}. \tag{11}$$

For complete orbits the number of diagonal elements is $4a$, because in a quantum states we have 4 nucleons with different spin and isospin projections. The number of diagonal terms for any kind of projectile nucleus is $N_1 = K$. One can obtain the first term of the generalized Bertsch correction by using the normalization factor for the harmonic oscillator wave function:

$$\langle \Psi_k | p_z^2 | \Psi_k \rangle_{\mathrm{diag}} = \frac{K}{A} \pi^{(a_A - a_K + \delta_{K,4a_K} - \delta_{A,4a_A})/4} \langle 0 | p_z^2 | 0 \rangle, \tag{12}$$

where $\delta_{A,4a_A}$ and $\delta_{K,4a_K}$ are Kronecker symbols corresponding to projectile respectively to the fragment having K nucleons.

The number of combinations between identical nucleons occupying the same cell from configuration space and having different projections of longitudinal momenta for ^{40}Ca nucleus type was in Bertsch theory a multiple of identical nucleon pairs in the projectile: $4A_a^2$. For a fragment with any number of nucleons K and a projectile with the mass number A, the total number of combination of this type is $N_2' = 2a_K(K - 2a_K - 2)$.

Let us consider the three-dimensional momentum space split up into a number of $(2q)^3$ Cartesian cells. The total number of combinations between identical nucleons having randomized momenta is then $C^2_{(2q)^3}$. We have to evaluate the number of nucleon pairs with aleator values for transverse components (p_x, p_y) in the projectile nucleus rest frame but also with longitudinal momenta coupled: $p_z \leftrightarrow (-p_z)$, $2p_z \leftrightarrow (-2p_z)$, $\ldots$, $qp_z \leftrightarrow (-qp_z)$. For each q value we have $(2q)^2$ transverse cells, so the number of possible pairs for a given interval $[kp_z; (k+1)p_z], \forall k = \overline{0,(q-1)}$ has to be $16q^4$. In order to obtain the physical real number of combinations between identical nucleons we have

$$N_2 = N_2' P(q) = 2a_K(K - 2a_K - 2) P(q), \tag{13}$$

with

$$P(q) = \frac{16q^5}{C^2_{(2q)^3}} = \frac{4q^2}{8q^3 - 1}. \tag{14}$$

Taking into account the anticorrelation between nucleon momenta, the evaluation of the second term of the dispersion gives (Ref. [6])

$$\langle \Psi | O_i O_j | \Psi \rangle_{\mathrm{id}} = \langle \Psi | f^2 p_z(-p_z) | \Psi \rangle_{\mathrm{id}} .$$

For the generalized case one can obtain

$$\langle \Psi_k | p_i p_j | \Psi_k \rangle_{\mathrm{id}} = -\frac{a_K^2 (K-2a_K-2)^2}{a_A^2 (A-2a_A-2)^2} \times \pi^{(a_A - a_K + \delta_{K,4a_K} - \delta_{A,4a_A})/4} \langle 0 | p_z^2 | 0 \rangle. \tag{15}$$

The factor N_3 represents the difference between the total number of possible nucleon-nucleon correlations A_{4a}^2 and the number of identical nucleons connections $4\ A_a^2$, i.e., $12\ a^2$. In general, for any light up to medium projectile and fragments

$$N_3 = 3a_K(a_K+1) + (K-a_K)(K-a_K-1). \tag{16}$$

Using the Goldhaber technique [3] in evaluating the last term of the quantum dispersion and neglecting the spatial correlations between identical nucleons, Bertsch reached the result below:

$$12a^2 \langle O_i O_k \rangle_{\mathrm{non}} \approx \frac{3K^2}{4} \langle p_i p_k \rangle_{\mathrm{non}} = -\frac{\langle 0 | p_z^2 | 0 \rangle}{3a} \frac{3K^2}{4}. \tag{17}$$

Following the same method as described in Refs. [3,6] and considering the mentioned correlations, the following can be obtained:

$$\langle \Psi_k | p_i p_j | \Psi_k \rangle_{\mathrm{non}} = \frac{-A + 2a_A(A-2a_A-2)P(q)}{3a_A(a_A+1) + (A-a_A)(A-a_A-1)} \times \langle 0 | p_z^2 | 0 \rangle. \tag{18}$$

C. The second order approximation for dispersion

In order to introduce the dependence of Fermi momenta on the temperature, it is useful to evaluate in the second order approximation the Fermi integral

$$I_F = \int_0^\infty G(\varepsilon) \frac{df_{\mathrm{FD}}}{d\varepsilon} d\varepsilon = \int_0^\infty g(\varepsilon) f_{\mathrm{FD}}(\varepsilon) d\varepsilon, \tag{19}$$

where $f_{\mathrm{FD}} = 1/(e^{\beta(\varepsilon-\mu)}+1)$ is Fermi-Dirac distribution function of fermions, $\beta = 1/k_B T$; the $G(\varepsilon)$ function obeys the condition $G(0)=0$ and $G(\varepsilon) = \int_0^\infty g(\varepsilon) d\varepsilon$.

The Fermi integral depends on the ς Riemann function of even arguments [36]:

$$I_F(\mu) = G(\mu) + 2\sum_{k=1}^{\infty} G^{2k}(\mu)(k_B T)^{2k} \left(1 - \frac{1}{2^{2k-1}}\right) \varsigma(2k), \tag{20}$$

$$\varsigma(2k) = \sum_{p=1}^{\infty} \frac{1}{p^{2k}} = \frac{2^{2k-1}}{(2k)!} \pi^{2k} B_k, \tag{21}$$

where B_k represents the tabled Bernoulli numbers: ($B_1 = \frac{1}{6}$; $B_2 = \frac{1}{30}$).

Using a finite number of terms of the sum, an approximate form of Fermi integral results as

$$I_F \approx G(\mu) + G^{(2)}(\mu)(k_B T)^2 \frac{\pi^2}{6} + G^{(4)}(\mu)(k_B T)^4 \frac{7\pi^4}{360}. \tag{22}$$

The last term adds an insignificant correction to the final result with respect to the experimental errors ($\leqslant 10^{-5}$ eV). Thus, we shall take the first two terms in order to evaluate the degree of the projectile excitation after the collision. The statistical media for the energy of fermions E_f and for the number of fermions N_f occupying a V volume and having each m_N mass, a spin $s = \frac{1}{2}$, and degeneracy factor $g_S = 2s+1$, are, respectively,

$$E_f = \frac{g_S V}{4\pi^2} \left(\frac{2m_N}{\hbar^2}\right)^{3/2} \int_0^\infty \frac{\varepsilon^{3/2}}{e^{\beta(\varepsilon-\mu)}+1} d\varepsilon, \tag{23}$$

$$N_f = \frac{g_S V}{4\pi^2} \left(\frac{2m_N}{\hbar^2}\right)^{3/2} \int_0^\infty \frac{\varepsilon^{1/2}}{e^{\beta(\varepsilon-\mu)}+1} d\varepsilon \approx \frac{V}{3\pi^2} \left(\frac{2m_N\mu}{\hbar^2}\right)^{3/2} \left[1 + \frac{\pi^2}{8} \left(\frac{k_B T}{\mu}\right)^2\right]. \tag{24}$$

TABLE II. The apparent excitation temperatures T [see Eq. (30)] of the $^{40}_{18}$Ar projectile associated with breakup into $^{16}_{8}$O and other residual fragments as compared with Goldhaber temperatures $T_{\mathrm{G\text{-}V}}$ [see Eq. (3)] on the experimental data of Viyogi and with the separation energies of the considered fragments per number of fragments.

σ_{0V} [a] (MeV/c)	q	T (MeV)	$T_{\mathrm{G\text{-}V}}$ [b] (MeV)	$\frac{E_{\mathrm{sep}}}{\text{No. of frag.}}$ (MeV)	Topology
				7.47	$^{40}_{18}\mathrm{Ar} \rightarrow {}^{16}_{8}\mathrm{O} + 5^4_2\alpha + 4^1_0 n$
	1	11.69 ± 3.94		9.56	$^{40}_{18}\mathrm{Ar} \rightarrow {}^{16}_{8}\mathrm{O} + 4^4_2\alpha + 2^3_1 t + 2^1_0 n$
78±8			6.65±1.36	10.70	$^{40}_{18}\mathrm{Ar} \rightarrow {}^{16}_{8}\mathrm{O} + 2^4_2\alpha + {}^{11}_{5}\mathrm{B} + {}^3_1 t + 2^1_0 n$
				10.71	$^{40}_{18}\mathrm{Ar} \rightarrow {}^{16}_{8}\mathrm{O} + {}^4_2\alpha + {}^{14}_{6}\mathrm{C} + {}^3_2\mathrm{He} + 3^1_0 n$
	2	17.23±3.71		9.61	$^{40}_{18}\mathrm{Ar} \rightarrow {}^{16}_{8}\mathrm{O} + {}^{22}_{10}\mathrm{Ne} + 2^1_0 n$
				13.33	$^{40}_{18}\mathrm{Ar} \rightarrow {}^{16}_{8}\mathrm{O} + {}^{20}_{9}\mathrm{F} + {}^3_1 t + {}^1_0 n$

[a]Reference [38].
[b]References [3,38].

TABLE III. The apparent excitation temperatures T [see Eq. (30)] of the $^{40}_{18}$Ar projectile associated with breakup into $^{20}_{9}$F and other residual fragments as compared with Goldhaber temperatures $T_{\mathrm{G\text{-}V}}$ [see Eq. (3)] on the experimental data of Viyogi and with the separation energies of the considered fragments per number of fragments.

σ_{0V} [a] (MeV/c)	q	T (MeV)	$T_{\mathrm{G\text{-}V}}$ [b] (MeV)	$\frac{E_{\mathrm{sep}}}{\text{No. of frag.}}$ (MeV)	Topology
				9.68	$^{40}_{18}\mathrm{Ar}\rightarrow{}^{20}_{9}\mathrm{F}+4^{4}_{2}\alpha+{}^{3}_{1}t+{}^{1}_{0}n$
				10.88	$^{40}_{18}\mathrm{Ar}\rightarrow{}^{20}_{9}\mathrm{F}+3^{4}_{2}\alpha+{}^{7}_{3}\mathrm{Li}+{}^{1}_{0}n$
	1	11.71±2.61		11.32	$^{40}_{18}\mathrm{Ar}\rightarrow{}^{20}_{9}\mathrm{F}+2^{4}_{2}\alpha+{}^{11}_{5}\mathrm{B}+{}^{1}_{0}n$
				13.12	$^{40}_{18}\mathrm{Ar}\rightarrow{}^{20}_{9}\mathrm{F}+2^{4}_{2}\alpha+{}^{10}_{4}\mathrm{Be}+{}^{2}_{1}d$
89±5			8.66±0.97	11.41	$^{40}_{18}\mathrm{Ar}\rightarrow{}^{20}_{9}\mathrm{F}+{}^{4}_{2}\alpha+{}^{15}_{7}\mathrm{N}+{}^{1}_{0}n$
				13.40	$^{40}_{18}\mathrm{Ar}\rightarrow{}^{20}_{9}\mathrm{F}+{}^{4}_{2}\alpha+{}^{14}_{6}\mathrm{C}+{}^{2}_{1}d$
				17.38	$^{40}_{18}\mathrm{Ar}\rightarrow{}^{20}_{9}\mathrm{F}+{}^{14}_{6}\mathrm{C}+{}^{6}_{3}\mathrm{Li}$
	2	18.05±2.46		17.50	$^{40}_{18}\mathrm{Ar}\rightarrow{}^{20}_{9}\mathrm{F}+{}^{20}_{9}\mathrm{F}$
				18.35	$^{40}_{18}\mathrm{Ar}\rightarrow{}^{20}_{9}\mathrm{F}+{}^{11}_{5}\mathrm{B}+{}^{9}_{4}\mathrm{Be}$
				19.90	$^{40}_{18}\mathrm{Ar}\rightarrow{}^{20}_{9}\mathrm{F}+{}^{10}_{5}\mathrm{B}+{}^{10}_{4}\mathrm{Be}$

[a]Reference [38].
[b]References [3,38].

Because the chemical potential of the fermions μ decreases very slowly with temperature for small T values one can adopt the ratio form $(k_BT/\varepsilon_F)\sim(k_BT/\mu)$, and can also be extracted the Fermi energy from Eq. (24), taking into account that for very small temperature values the superior limit of the integral is ε_F and the Fermi-Dirac function turns into step function $f_{\mathrm{FD}}(\varepsilon)\rightarrow\Theta_{\mathrm{H}}(\mu-\varepsilon)$:

$$\varepsilon_F=\frac{\hbar^2}{2m_N}\left(\frac{3\pi^2N}{V}\right)^{2/3}. \tag{25}$$

In order to evaluate the fermionic energy per nucleon and respectively the dispersion of nucleon momenta in the rest frame of the fragmenting nucleus one needs to introduce Eq. (22) in Eq. (23), to neglect the terms $\propto T^4$, and to use the Taylor first order approximation for $x\rightarrow 0$: $(1+x)^{\alpha}\approx 1+\alpha x$

$$E_f=\frac{3\mu N_f}{5}\frac{1+\frac{5\pi^2}{8}\left(\frac{k_BT}{\varepsilon_F}\right)^2}{1+\frac{\pi^2}{8}\left(\frac{k_BT}{\varepsilon_F}\right)^2}\approx\frac{3\varepsilon_FN_f}{5}\left[1-\frac{\pi^2}{12}\left(\frac{k_BT}{\varepsilon_F}\right)^2\right]\times\left[1+\frac{\pi^2}{2}\left(\frac{k_BT}{\varepsilon_F}\right)^2\right], \tag{26}$$

$$\sigma^2_{0\mathrm{theor}}(T)=\frac{\langle p^2\rangle}{3}\approx\frac{p_F^2}{5}\left[1+\frac{5\pi^2}{12}\left(\frac{k_BT}{\varepsilon_F}\right)^2\right]. \tag{27}$$

We use from now on the natural system of units ($\hbar=c=k_B=1$) and take into account the Bertsch generalized correction for any light and medium projectile nuclei where the approximation of harmonic oscillator wave function is considered. We also apply the Murphy correction, where the

TABLE IV. The apparent excitation temperatures T [see Eq. (30)] of the $^{40}_{18}$Ar projectile associated with breakup into $^{25}_{12}$Mg and other residual fragments as compared with Goldhaber temperatures $T_{\mathrm{G\text{-}V}}$ [see Eq. (3)] on the experimental data of Viyogi and with the separation energies of the considered fragments per number of fragments.

σ_{0V} [a] (MeV/c)	q	T (MeV)	$T_{\mathrm{G\text{-}V}}$ [b] (MeV)	$\frac{E_{\mathrm{sep}}}{\text{No. of frag.}}$ (MeV)	Topology
				7.62	$^{40}_{18}\mathrm{Ar}\rightarrow{}^{25}_{12}\mathrm{Mg}+3^{4}_{2}\alpha+3^{1}_{0}n$
				10.78	$^{40}_{18}\mathrm{Ar}\rightarrow{}^{25}_{12}\mathrm{Mg}+2^{4}_{2}\alpha+2^{3}_{1}t+{}^{1}_{0}n$
				11.24	$^{40}_{18}\mathrm{Ar}\rightarrow{}^{25}_{12}\mathrm{Mg}+{}^{4}_{2}\alpha+{}^{10}_{4}\mathrm{Be}+{}^{1}_{0}n$
90±5	1	12.85±2.47	8.85±0.98	12.44	$^{40}_{18}\mathrm{Ar}\rightarrow{}^{25}_{12}\mathrm{Mg}+{}^{4}_{2}\alpha+{}^{7}_{3}\mathrm{Li}+{}^{3}_{1}t+{}^{1}_{0}n$
				10.98	$^{40}_{18}\mathrm{Ar}\rightarrow{}^{25}_{12}\mathrm{Mg}+{}^{14}_{6}\mathrm{C}+{}^{1}_{0}n$
				13.04	$^{40}_{18}\mathrm{Ar}\rightarrow{}^{25}_{12}\mathrm{Mg}+4^{3}_{1}t+2^{1}_{1}p+{}^{1}_{0}n$
				13.39	$^{40}_{18}\mathrm{Ar}\rightarrow{}^{25}_{12}\mathrm{Mg}+{}^{11}_{5}\mathrm{B}+{}^{3}_{1}t+{}^{1}_{0}n$

[a]Reference [38].
[b]References [3,38].

TABLE V. The apparent excitation temperatures T [see Eq. (30)] of the $^{40}_{18}$Ar projectile associated with breakup into $^{30}_{14}$Si and other residual fragments as compared with Goldhaber temperatures $T_{\text{G-V}}$ [see Eq. (3)] on the experimental data of Viyogi and with the separation energies of the considered fragments per number of fragments.

σ_{0V} [a] (MeV/c)	q	T (MeV)	$T_{\text{G-V}}$ [b] (MeV)	$\frac{E_{\text{sep}}}{\text{No. of frag.}}$ (MeV)	Topology
	2	9.09±2.71		6.32	$^{40}_{18}\text{Ar}\rightarrow ^{30}_{14}\text{Si}+2^{4}_{2}\alpha+2^{1}_{0}n$
				10.28	$^{40}_{18}\text{Ar}\rightarrow ^{30}_{14}\text{Si}+^{4}_{2}\alpha+^{3}_{1}t+^{1}_{1}p+2^{1}_{0}n$
92±5			9.25±1.01	10.73	$^{40}_{18}\text{Ar}\rightarrow ^{30}_{14}\text{Si}+^{4}_{2}\alpha+2^{3}_{1}t$
	3	13.10±2.33		11.61	$^{40}_{18}\text{Ar}\rightarrow ^{30}_{14}\text{Si}+^{10}_{4}\text{Be}$
				12.55	$^{40}_{18}\text{Ar}\rightarrow ^{30}_{14}\text{Si}+3^{3}_{1}t+^{1}_{1}p$

[a]Reference [38].
[b]References [3,38].

nucleons in the fragment nucleus are supposed to have Fermi distribution. Thus, the width of Fermi nucleon momenta distribution soon after the collision took place is given by [37]

$$\sigma_0 = C_M C_B \frac{p_F}{\sqrt{5}} \sqrt{1+\frac{5\pi^2}{12}\left(\frac{2m_N T}{p_F^2}\right)^2}, \tag{28}$$

where $m_N = 938$ MeV, $C_M = (w'/w)_M$,

$$C_B^{-2} = \left(\frac{\sigma_G}{\sigma_B}\right)^2 = \frac{N_G B_{\text{diag}}}{N_1 B_{\text{diag}} + N_2 B_{\text{id}} + N_3 B_{\text{non}}} \tag{29}$$

where $B_{\text{diag}} = \langle \Psi_k | p_z^2 | \Psi_k \rangle_{\text{diag}}$, $B_{\text{id}} = \langle \Psi_k | p_i p_j | \Psi_k \rangle_{\text{id}}$, $B_{\text{non}} = \langle \Psi_k | p_i p_j | \Psi_k \rangle_{\text{non}}$.

One can determine the apparent temperature as a function of the percentage of the nucleons having the same spin and isospin and anticorrelated projected momenta on the incident axis in the projectile rest frame:

$$T = \frac{p_F^2}{\pi m_N} \sqrt{3\left[\left(\frac{w}{w'}\right)_M^2 \left(\frac{\sigma_0}{p_F}\right)^2 \left(\frac{\sigma_G}{\sigma_B}\right)^2 - \frac{1}{5}\right]}. \tag{30}$$

IV. RESULTS AND DISCUSSION

The apparent excitation temperatures T of the $^{40}_{18}$Ar projectile corresponding to different breakup modes were calculated according to Eq. (30) from the experimental widths obtained by Viyogi *et al.* (Ref. [38]). Finally, we compared them with Goldhaber temperatures $T_{\text{G-V}}$ [Eq. (3)] on the same data and with the separation energies of the considered fragments per number of fragments (see Tables II–VI).

It can be observed that the degree of projectile fragmentation increases with the apparent excitation temperature and with the number of possible states in the momentum space. The analyzed fragmentation topology clearly shows a dependence of the received energy on the number of α released as confirmed in nuclear emulsion experiments [39].

Another interesting remark regards the obtained minimum q value for the fragmentation modes $^{40}_{18}\text{Ar}\rightarrow ^{36}_{16}\text{S}+\cdots$. For other topological modes corresponding to an equal number of one-dimensional momentum cells 2 q, the apparent temperature would be substantially greater. One deduces from the Heisenberg uncertainty relations ($\Delta z \geqslant \hbar/\Delta p_z$) that the dimension of the coordinate cell for the above breakup would also be higher. That indicates a smaller degree of excitation after the collision as expected, proving that the theory is self-consistent.

TABLE VI. The apparent excitation temperatures T [see Eq. (30)] of the $^{40}_{18}$Ar projectile associated with breakup into $^{36}_{16}$S and other residual fragments as compared with Goldhaber temperatures $T_{\text{G-V}}$ [see Eq. (3)] on the experimental data of Viyogi and with the separation energies of the considered fragments per number of fragments.

σ_{0V} [a] (MeV/c)	q	T (MeV)	$T_{\text{G-V}}$ [b] (MeV)	$\frac{E_{\text{sep}}}{\text{No. of frag.}}$ (MeV)	Topology
	3	5.90±3.07		3.41	$^{40}_{18}\text{Ar}\rightarrow ^{36}_{16}\text{S}+^{4}_{2}\alpha$
94±5			9.66±1.03	7.02	$^{40}_{18}\text{Ar}\rightarrow ^{36}_{16}\text{S}+2^{1}_{1}p+2^{1}_{0}n$
	4	8.41±2.37		8.87	$^{40}_{18}\text{Ar}\rightarrow ^{36}_{16}\text{S}+^{3}_{1}t+^{1}_{1}p$
				9.13	$^{40}_{18}\text{Ar}\rightarrow ^{36}_{16}\text{S}+^{3}_{2}\text{He}+^{1}_{0}n$

[a]Reference [38].
[b]References [3,38].

By considering the interaction between projectile and target, we found that the Fermi distribution has changed. Consequently, one can notice that the width of the momentum distribution for $^4He+^7Li$ interactions as measured in the fragmenting nucleus rest frame has increased and also that the average momentum has decreased. Therefore, we believe that the Goldhaber formula [Eq. (2)] could be applied only for the fragmenting channels which implies a very small transfer of energy and momentum ($T\rightarrow 0$), or in the fragmentation of neutron-rich projectiles, where a surviving prefragment can be observed (see Refs. [40,41]). As for those fragmenting channels that are strongly affected by the interaction at the interface between projectile and target, the Goldhaber formula underestimates the mean square momenta of the fragments and Eq. (30) should be applied.

Still, a contribution of the evaporation phase to the observed mass loss is a correction that one needs to consider further in studying heavy projectile fragmentation process where the so-called ''memory effect'' is no longer visible [42,43]. In this case, a higher excitation of the projectile during the formation of neutron-deficient fragments is implied by the dependence of the production yields on the neutron excess of the projectile with respect to the line of β-stability [44].

V. CONCLUSIONS

The results seem to point out a dependence of the projectile degree of excitation soon after nuclear collision occurred on the breakup topology. The width of the longitudinal momenta distribution as measured in the projectile rest frame was found to be closely linked to the projectile-target overlapping degree (Fig. 6). The estimator chosen for the presented analysis was the apparent temperature associated to a possible state of thermal equilibrium even though it was used on a nuclear fragmenting system having small (^4He) or relative small number of nucleons (^{40}Ar).

The Goldhaber formula was thus improved by corroborating the projectile excitation hypothesis [15] with two corrections proposed by Bertsch and Murphy [6,7], and by using the probability that identical nucleons having anticorrelated momenta to be close together in the coordinate space. We found apparent temperature values corresponding to a large variety of breakup channels by combining Eq. (2) with Eq. (28).

Nevertheless, the applicability of the model described in this paper is limited for light up to medium nuclei where one expects to use harmonic oscillator wave function. As for heavy ion interactions, the model should provide radial flow calculations. The treatment of the projectile fragmentation sequential process requires also further investigation.

ACKNOWLEDGMENTS

The authors wish to express their gratitude to SKM 200 Collaboration, especially to E. O. Okonov and G. L. Vardenga from the Joint Institute for Nuclear Research – Dubna (Russia). We are indebted to H. Sorge for running RQMD 2.4 calculations. The authors would also like to thank V. Popa, L. Popa, M. Haşegan, C. Vaman, and R. Mărginean for helpful discussions and comments on this paper.

[1] H. H. Heckman *et al.*, in *Proceedings of the 5th International Conference on High Energy Physics and Nuclear Structure*, Uppsala, Sweden, 1973, edited by G. Tibbell (Elsevier, New York, 1974), p. 403.
[2] H. Feshbach and K. Huang, Phys. Lett. **47B**, 300 (1973).
[3] A. S. Goldhaber, Phys. Lett. **53B**, 306 (1974).
[4] J. V. Lepore and R. J. Riddell, Jr., LBL Report LBL-3086 (1974); in Proceedings, Lawrence Berkeley Lab. Lbl.-3675, 283 (1974).
[5] D. E. Greiner, P. J. Lindstrom, H. H. Heckman, B. Cork, and F. S. Bieser, Phys. Rev. Lett. **35**, 152 (1975).
[6] G. F. Bertsch, Phys. Rev. Lett. **46**, 472 (1981).
[7] M. J. Murphy, Phys. Lett. **135B**, 25 (1984).
[8] H. H. Gan, S. J. Lee, S. Das Gupta, and J. Barrette, Phys. Lett. B **234**, 4 (1990).
[9] F. P. Brady *et al.*, Phys. Rev. Lett. **60**, 1699 (1988), and references given therein.
[10] J. Dreute, W. Heinrich, G. Rusch, and B. Wiegel, Phys. Rev. C **44**, 1057 (1991).
[11] H. H. Heckman, D. E. Greiner, P. J. Lindstrom, and F. S. Bieser, Phys. Rev. Lett. **28**, 926 (1972).
[12] M. Muthuswamy, E814 Collaboration, Nucl. Phys. **A544**, 423c (1992).
[13] A. Schüttauf *et al.*, Nucl. Phys. **A607**, 457 (1996).
[14] G. M. Chernov, K. G. Gulamov, U. G. Gulyamov, V. Sh. Navotny, N. V. Petrov, L. N. Svechnikova, B. Jakobsson, A. Oskarsson, and I. Otterlund, Nucl. Phys. **A412**, 534 (1984).
[15] W. Bauer, Phys. Rev. C **51**, 803 (1995).
[16] P. B. Gossiaux, R. Puri, Ch. Hartnack, and J. Aichelin, Nucl. Phys. **A619**, 379 (1997).
[17] A. S. Botvina *et al.*, Nucl. Phys. **A584**, 737 (1995).
[18] S. Albergo *et al.*, Nuovo Cimento A **89**, 1 (1985).
[19] A. Kolomiets *et al.*, Phys. Rev. C **54**, R472 (1996).
[20] M. J. Huang *et al.*, Phys. Rev. Lett. **78**, 1648 (1997).
[21] F. Gulminelli and D. Durand, Nucl. Phys. **A615**, 117 (1997).
[22] J. P. Bondorf, A. S. Botvina, and I. N. Mishustin, Phys. Rev. C **58**, 27 (1998).
[23] V. Serfling *et al.*, Phys. Rev. Lett. **80**, 3928 (1998).
[24] D. J. Morrissey *et al.*, Annu. Rev. Nucl. Part. Sci. **44**, 65 (1994).
[25] J. Pochodzalla *et al.*, Phys. Rev. C **35**, 1695 (1987).
[26] G. J. Kunde *et al.*, Phys. Lett. B **272**, 202 (1991).
[27] C. Besliu and Al. Jipa, Rom. J. Phys. **37**, 1011 (1992).
[28] A. U. Abdurakhimov *et al.*, Nucl. Phys. **A362**, 376 (1981).
[29] V. D. Aksinenko *et al.*, Nucl. Phys. **A348**, 518 (1980).
[30] V. D. Aksinenko *et al.*, Nucl. Phys. **A324**, 266 (1979).

[31] O. Benary, R. Price, and G. Alexander, UCRL-20000 NN report (1970).
[32] R. Hagedorn, in *Relativistic Kinematics*, edited by John David Jackson and David Pines (W. A. Benjamin, New York, 1963), p. 46.
[33] P. R. Bevington and D. K. Robinson, in *Data Reduction and Error Analysis for the Physical Sciences*, edited by Susan J. Tubb and John M. Morris (McGraw-Hill, New York, 1992), p. 75.
[34] O. Sima, in *Simularea Monte Carlo a Transportului Radiaţiilor*, edited by C. Pioaru, S. Stanciu, and C. Fraţila (Ed. ALL, Bucharest, 1994), p. 23.
[35] E. J. Moniz, I. Sick, R. R. Whitney, J. R. Ficenec, R. D. Kephart, and W. P. Trower, Phys. Rev. Lett. **26**, 445 (1971).
[36] L. D. Landau and E. M. Lifchitz, in *Fizica Statistică*, 5th vol., 3rd ed., edited by R. Dinu, O. Nistor, and S. Dumitrescu (Ed. Tehnică, Bucharest, 1988), translation by G. Ciobanu and N. Fiuciuc after *Statisticeskaya Fizika*, tom V (Ed. Nauka, Moskow, 1978), p. 160.
[37] D. Felea, C. Besliu, V. Topor-Pop, A. Gheata, Al. Jipa, I.-S. Zgura, and R. Zaharia, in the 36th course of the International School of Subnuclear Physics, Erice-Sicily, Italy, 1998 (oral presentation); in *Proceedings of the 8th International Conference on the Structure of Baryons-Baryons '98*, Bonn, Germany, 1998 (World Scientific, Singapore, 1999), p. 705.
[38] Y. P. Viyogi *et al.*, Phys. Rev. Lett. **42**, 33 (1979).
[39] B. Jakobsson, R. Kullberg, and I. Otterlund, Lett. Nuovo Cimento **15**, 444 (1976).
[40] K.-H. Schmidt *et al.*, Nucl. Phys. **A542**, 699 (1992).
[41] E. Hanelt *et al.*, Z. Phys. A **346**, 43 (1993).
[42] C. Donzaud *et al.*, Nucl. Phys. **A593**, 503 (1995).
[43] J. Reinhold, J. Friese, H.-J. Körner, R. Schneider, K. Zeitelhack, H. Geissel, A. Magel, G. Münzenberg, and K. Sümmerer, Phys. Rev. C **58**, 247 (1998).
[44] J. Friese *et al.*, Nucl. Phys. **A553**, 735c (1993).